



1 **Dust pollution substantially weakens the impact of ammonia**
2 **emission reduction on particulate nitrate formation**

3 Hanrui Lang¹, Yunjiang Zhang^{1*}, Sheng Zhong², Yongcai Rao³, Minfeng Zhou⁴, Jian Qiu⁵, Jingyi Li¹, Diwen Liu⁶, Florian
4 Couvidat⁷, Olivier Favez⁷, Didier Hauglustaine⁸, Xinlei Ge¹

5 ¹Collaborative Innovation Center of Atmospheric Environment and Equipment Technology, Jiangsu Key Laboratory of
6 Atmospheric Environment Monitoring and Pollution Control, Nanjing University of Information Science and Technology,
7 Nanjing, China

8 ²Jiangsu Environmental Monitoring Center, Nanjing, China

9 ³Xuzhou Environmental Monitoring Center of Jiangsu, Xuzhou, China

10 ⁴Suzhou Environmental Monitoring Center of Jiangsu, Suzhou, China

11 ⁵Zhenjiang Environmental Monitoring Center of Jiangsu, Zhenjiang, China

12 ⁶Graduate School of Arts and Science, Columbia University, New York City, USA

13 ⁷Institut National de l'Environnement Industriel et des Risques, Verneuil-en-Halatte, France

14 ⁸Laboratoire des Sciences du Climat et de l'Environnement, CNRS-CEA-UVSQ, Université Paris-Saclay, Gif-sur-Yvette,
15 France

16 *Correspondence to:* Yunjiang Zhang (yjzhang@nuist.edu.cn)

17



18 **Abstract.** Dust emissions significantly influence air quality and contribute to nitrate aerosol pollution by altering aerosol
19 acidity. Understanding how dust interacts with ammonia emission controls is crucial for managing particulate nitrate
20 pollution, especially in urban areas. In this study, we conducted field measurements of aerosol components and gases
21 across three cities in Eastern China during the spring of 2023. By combining an aerosol thermodynamic model with
22 machine learning, we assessed the contribution of dust to aerosol pH and its impact on nitrate formation. Our results show
23 that changes in ammonia, both in the gas and particle phases, were the main factors affecting aerosol pH, with dust
24 particles contributing to about 7% of the total pH variation. During dust events, high concentrations of non-volatile ions
25 increased aerosol pH, leading to higher nitrate levels in particulate form. Machine learning analysis revealed that extreme
26 dust storms caused a significant change in aerosol pH, enhancing nitrate partitioning. Further simulations indicated that
27 while reducing ammonia emissions is effective in lowering nitrate levels under normal conditions, this effect is
28 significantly reduced in dust-affected environments. Dust particles act as a buffer, reducing the sensitivity of nitrate
29 formation to ammonia emission reductions. These findings emphasize the need to consider dust pollution when designing
30 strategies for controlling particulate nitrate levels and highlight the complex interactions between dust and anthropogenic
31 emissions.

32



33 1 Introduction

34 Airborne dust is a major component of atmospheric aerosols, accounting for approximately 75% of the global aerosol
 35 mass load (Mahowald et al., 2006; Zhao et al., 2022; Chen et al., 2023c). Dust exerts multiple impacts on air quality
 36 (Jickells et al., 2005; Rosenfeld et al., 2001), climate (Huang et al., 2011), and human health (Zhang et al., 2023; Goudie,
 37 2014). It can be broadly categorized into anthropogenic dust and natural dust based on sources and emission mechanisms
 38 (Chen et al., 2018; Chen et al., 2023a). Anthropogenic dust originates from human activities, such as construction,
 39 agricultural and non-exhaust vehicular emissions (Liu et al., 2021). In contrast, natural dust mainly arises from bare
 40 surfaces in arid and semi-arid regions (Shao and Dong, 2006), which cover approximately 30% of the global land area
 41 (Soussé-Villa et al., 2024; Xin et al., 2023). Beyond anthropogenic influences, over 300 countries worldwide are affected
 42 by natural dust pollution (Kurokawa and Ohara, 2020; Notaro et al., 2015). Dust storms originating in arid regions can be
 43 transported over thousands of kilometers, significantly impacting downstream air quality and atmospheric chemistry (Tan
 44 et al., 2012; Milousis et al., 2024; Sun et al., 2001).

45 Dust emissions contain nonvolatile cations (NVCs), such as calcium and magnesium ions, which are alkaline substances
 46 that can neutralize acidic aerosol components, such as sulfates, thereby increasing aerosol pH (Wu et al., 2013; Ding et
 47 al., 2019). Dust particles also engage in heterogeneous reactions with gaseous nitric acid, buffering acidic species and
 48 modulating pH dynamics. Aerosol pH is a critical factor in atmospheric chemical processes, influencing gas-particle
 49 partitioning of inorganic aerosols (Guo et al., 2018), secondary organic aerosol (SOA) formation (Xu et al., 2015; Zhang
 50 et al., 2017; Nguyen et al., 2014), and metal-catalyzed oxidation reactions (Fang et al., 2017). Regional variations in
 51 aerosol pH alter the chemical characteristics of atmospheric pollution, affecting pollutant lifetimes and deposition rates,
 52 which in turn have profound implications for ecosystems and public health (Guo et al., 2016). Despite the incorporation
 53 of aerosol pH modules in some atmospheric chemistry models, inaccuracies in dust emission inventories can lead to biases
 54 in estimated aerosol pH, thereby introducing systematic errors in simulating associated chemical processes, such as nitrate
 55 formation.

56 Nitrate has emerged as a dominant component of fine particulate matter (PM_{2.5}) worldwide (e.g., China, Europe, the
 57 United States, and India), particularly as sulfate aerosol concentrations decline due to sustained SO₂ emission reductions
 58 (Weber et al., 2016; Geng et al., 2017; Zhai et al., 2021; Hauglustaine et al., 2014; Beaudor et al., 2024). The reaction
 59 between gaseous nitric acid (HNO₃) and ammonia (NH₃) represents one of the primary pathways for the formation of fine
 60 mode nitrate (Stelson and Seinfeld, 1982; Metzger et al., 2002). Nitrate formation plays a critical role in atmospheric



61 chemistry and the global nitrogen cycle, including reactive nitrogen deposition (Chul H. Song, 2000). The gas-particle
 62 partitioning of HNO_3 and nitrate formation is strongly influenced by aerosol pH (Guo et al., 2018; Shi et al., 2019). When
 63 total ammonia (gaseous and particulate) or NVCs are insufficient to fully neutralize aerosol sulfate, HNO_3 will not
 64 condense on aerosol due to low pH (Nenes et al., 2020; Guo et al., 2017a; Vasilakos et al., 2018; Ding et al., 2019).
 65 However, this conceptual framework may oversimplify the influence of aerosol acidity, as it fails to fully consider the
 66 substantial volatility differences between deliquescent aerosols containing sulfates or NVCs and those dominated by
 67 ammonium or nitrate, both of which are highly sensitive to aerosol pH (Nenes et al., 2020; Nenes et al., 2021). In dust-
 68 polluted environments, however, the abundance of alkaline particles, such as calcium ions, can alter nitrate formation
 69 pathways (Seinfeld et al., 1998; Hrdina et al., 2021; Li et al., 2024). Quantitative insights into how urban dust influences
 70 nitrate formation and its regulation remain nevertheless limited.

71 East Asia, home to some of the world's major dust source regions, significantly contributes to global atmospheric dust
 72 pollution. Under the influence of Mongolian cyclones, dust particles originating from Mongolia are transported long
 73 distances, affecting air quality and atmospheric processes across East Asia (Fu et al., 2014; Sun et al., 2001; Wang et al.,
 74 2021). The Yangtze River Delta (YRD) is a densely urbanized region in Eastern China, where air quality is influenced by
 75 both natural and local anthropogenic dust sources. This region provides an ideal atmospheric setting to investigate the
 76 impact of dust pollution on urban aerosol acidity and nitrate chemistry. Under these contexts, this study examines changes
 77 in aerosol pH, and nitrate gas-particle partitioning (defined as the gas-particle partitioning of HNO_3 combined to its acid
 78 dissociation) under influence of both anthropogenic and natural dust pollution in spring 2023, focusing on three
 79 representative cities (Xuzhou, Zhenjiang, and Suzhou) in the YRD. The contributions of chemical and meteorological
 80 components to aerosol pH and the effects of dust storms on $\varepsilon(\text{NO}_3^-)$ are quantified. By integrating statistical analysis
 81 approaches, we further quantify the contribution of different factors to aerosol pH and $\varepsilon(\text{NO}_3^-)$. Sensitivity analyses are
 82 conducted to evaluate the effects of TNH_x ($\text{TNH}_x = \text{NH}_3 + \text{NH}_4^+$), TNO_3 ($\text{TNO}_3 = \text{HNO}_3 + \text{NO}_3^-$) and SO_4^{2-} emission
 83 controls on nitrate partitioning across varying dust pollution levels, providing a scientific basis for formulating nitrate
 84 pollution control strategies during dust events.

85 **2.Data and Methods**

86 **2.1 Sampling site and instruments**

87 This study selected three cities in the YRD region, China, that represent a gradient of dust transport effects: Xuzhou



88 (32.18°N, 119.48°E), Zhenjiang (32.16°N, 119.49°E), and Suzhou (31.29°N, 120.61°E). These cities are distributed along
 89 the north-to-south dust transport pathway, enabling a systematic investigation of the impacts of dust transport, including
 90 gradient variations in particle chemical properties, aerosol acidity (pH), and gas–particle partitioning. The sampling sites
 91 comprehensively reflect the gradient effects of dust across different regions. Observations were conducted at
 92 environmental monitoring stations within each city. These urban monitoring sites, located in mixed residential and
 93 commercial areas, are influenced by multiple sources, including industrial and traffic emissions (Zheng et al., 2021).
 94 Water-soluble inorganic ions in PM_{2.5} (e.g., NH₄⁺, Na⁺, K⁺, Ca²⁺, Mg²⁺, SO₄²⁻, NO₃⁻, Cl⁻) and gaseous components (NH₃,
 95 HNO₃, HCl) were continuously monitored using a Monitor for AeRosols and Gases in ambient Air (MARGA) system
 96 (Trebs et al., 2004; Rumsey et al., 2014). The system exhibited high correlation between cation and anion measurements
 97 (Fig. S1). Throughout the monitoring period, ambient air samples were drawn into the system, where aerosols and gaseous
 98 pollutants were separated. Aerosol particles were collected using a wet sampler, dissolved in water to form sample liquid,
 99 and then analyzed via ion chromatography. For gaseous pollutants, air samples passed through a membrane filter to
 100 remove particles before entering a scrubbing tower, where gas-phase components were dissolved in water to form sample
 101 liquid for ion chromatographic analysis (Rumsey et al., 2014). The MARGA system is equipped with automatic
 102 calibration and cleaning functions, ensuring stability and accuracy during long-term operation. The entire process is
 103 controlled by dedicated software, enabling simultaneous monitoring of multiple components and real-time data output
 104 (Schaap et al., 2004). Meteorological data (temperature and relative humidity) were obtained from corresponding
 105 observation stations, while additional meteorological parameters were sourced from the European Centre for Medium-
 106 Range Weather Forecasts (ECMWF) ERA5 reanalysis dataset (<https://cds.climate.copernicus.eu/>, last access: November
 107 21, 2023). Regional PM₁₀ data were retrieved from the China National Environmental Monitoring Centre
 108 (<https://air.cnemc.cn:18007/>, last access: November 21, 2023).

109 2.2 Aerosol pH estimation

110 Aerosol pH is a particle property that significantly influences aerosol formation, yet it is challenging to measure directly.
 111 Traditional methods, such as ion balance and molar ratio approaches, often fail to provide accurate evaluations of aerosol
 112 pH (Guo et al., 2016; Weber et al., 2016). Currently, the most widely used approaches include the ISORROPIA-II
 113 thermodynamic model (Fountoukis and Nenes, 2007). In this study, we employed the ISORROPIA-II thermodynamic
 114 model to estimate aerosol pH (see Eq. 1) as well as the gas–particle partitioning of water-soluble ions, semi-volatile



compounds, and water content. At low RH, aerosols are unlikely to be in a completely liquid state, and secondary organic aerosols (SOA) may affect the distribution of semi-volatile compounds due to reduced diffusion within the particles, thus influencing the predicted pH values; At high RH levels, such as $RH > 95\%$, aerosols may deliquesce, and the exponential increase in water activity (W_i) can introduce significant uncertainty into the pH values (Guo et al., 2017b; Malm and Day, 2001). To improve the model's accuracy, we applied both the forward mode for metastable aerosols and excluded data with relative humidity (RH) below 35% or above 95% (Nah et al., 2018; Guo et al., 2015). The equation used to calculate aerosol pH in ISORROPIA-II is as follows (Liu et al., 2022):

$$pH = -\log_{10} \frac{1000\gamma_{H^+}C_{H^+}}{W_i} \quad (1)$$

In the Eq. (1), γ_{H^+} represents the activity coefficient of hydrogen ions, which is generally set to 1 (Liu et al., 2022). C_{H^+} denotes the hydrogen ion concentration in the aerosol aqueous phase, expressed in $\mu\text{g m}^{-3}$. W_i refers to the water content of the aerosol phase output by ISORROPIA-II (in $\mu\text{g m}^{-3}$). By incorporating these parameters, the ISORROPIA-II model provides a reliable framework for estimating aerosol pH, allowing for accurate analysis of its variation and impact under different environmental and pollution scenarios, including those influenced by dust events.

2.3 The gas–particle partitioning of nitrate ($\varepsilon(\text{NO}_3^-)$)

Nitrate, owing to its volatility, exists in the atmosphere in two primary forms. In the particulate phase, it predominantly appears as semi-volatile ammonium nitrate. However, where ammonia and NVCs fail to fully neutralize aerosol sulfate, the formation of semi-volatile ammonium nitrate is inhibited. Under such conditions, nitrate tends to remain in the gaseous phase as HNO_3 , which can subsequently transform into more stable coarse-mode salts, such as $\text{Ca}(\text{NO}_3)_2$, over time (Guo et al., 2017c; Vasilakos et al., 2018; Hrdina et al., 2021). $\varepsilon(\text{NO}_3^-)$ defined as the ratio between particle-phase nitrate over TNO_3 serves as a key indicator of nitrate distribution between its gaseous and particulate phases. Changes in aerosol pH, influenced by varying meteorological conditions, significantly affect $\varepsilon(\text{NO}_3^-)$. This study employs Eq. (2) (Guo et al., 2018; Nenes et al., 2020) to calculate theoretical values of $\varepsilon(\text{NO}_3^-)$ for each observational dataset. The results enable a detailed analysis of how variations in pH across different ranges influence the gas–particle partitioning of nitrate.

$$\varepsilon(\text{NO}_3^-) = \frac{H_{\text{HNO}_3}^* W_i RT (0.987 \times 10^{-14})}{\gamma_{\text{NO}_3^-} \gamma_{H^+} 10^{-pH} + H_{\text{HNO}_3}^* W_i RT (0.987 \times 10^{-14})} \quad (2)$$

In the equation, $H_{\text{HNO}_3}^* = H_{\text{HNO}_3} K_{a1}$ ($\text{mol}^2 \text{ kg}^{-2} \text{ atm}^{-1}$) represent the product of the Henry's law constant and the acid dissociation constant for HNO_3 . R is the ideal gas constant ($\text{J mol}^{-1} \text{ K}^{-1}$), and T is the temperature in Kelvin (K). The



141 temperature dependence for H_{HNO_3} and K_{n1} can be found in Clegg et al. (1998). pH is calculated using Eq. (1). The factor
 142 0.987×10^{-14} is a unit conversion factor used to convert from atm and μg to SI units. $\gamma_{NO_3^-}$ and γ_{H^+} are the activity
 143 coefficients for NO_3^- and H^+ , respectively. Activity coefficient predicted by ISORROPIA-II are $\gamma_{NO_3^-}\gamma_{H^+}=0.28$, $\gamma_{H^+}=1$
 144 (Guo et al., 2018; Guo et al., 2017b; Nah et al., 2018). In the standard S-curve, pH varies within a specific range, and this
 145 relationship is influenced by the temperature dependence of the Henry's law constant and the acid dissociation constant.
 146 This model allows for a more accurate estimation of nitrate aerosol behavior under varying environmental conditions.
 147 More detailed information about inputs and outputs for the ISORROPIA-II model can be found in Tables S1 – S3.

148 **2.4 Multi-site concentration weighted trajectory (CWT)**

149 The CWT analysis method is widely used to assess the potential origins and transport pathways of air pollutants observed
 150 at receptor sites. By integrating trajectory analysis, this approach provides insights into pollutant sources and their
 151 atmospheric transport dynamics. In this study, we employed the CWT model, coupled with backward trajectories and
 152 multi-site air quality monitoring data, to investigate the potential source regions and long-range transport of the spring
 153 2023 dust storm event observed in Xuzhou, Zhenjiang, and Suzhou. When combined with data from multiple monitoring
 154 sites, the CWT model demonstrates enhanced robustness and reliability (Boichu et al., 2019). Briefly, multi-site CWT
 155 analysis integrates pollutant concentration data from several monitoring stations with the corresponding backward
 156 trajectories to estimate the likely origins of the observed pollutants. Air pollutant concentrations are spatially allocated to
 157 grid cells traversed by air masses, weighted by the residence time within each grid cell. Compared to single-site CWT
 158 analysis, the multi-site approach offers broader spatial coverage, minimizes site-specific biases, and increases the dataset
 159 size, thereby improving the accuracy and spatial resolution of source apportionment, particularly for complex transport
 160 patterns.

161 In this study, 48-hour backward trajectories at 50 meters above ground level were computed using meteorological data
 162 from the Global Data Assimilation System (GDAS). The CWT analysis was conducted using the Zefir toolkit
 163 implemented in Igor Pro (Petit et al., 2017). This methodology provided a comprehensive assessment of dust transport
 164 and source attribution, facilitating a deeper understanding of dust storm dynamics in the region.

$$165 \quad CWT_{ij} = \frac{\sum_{l=1}^n C_l \tau_{ij,l}}{\sum_{l=1}^n \tau_{ij,l}} \quad (3)$$

166 In Eq. (3), CWT_{ij} represents the weighted concentration in the grid at the i row and j column, C_l is the pollutant



167 concentration corresponding to the l trajectory, and $\tau_{ij,l}$ is the residence time of the trajectory in the (ij) grid. n denotes
 168 the total number of all trajectories.

169 2.5 Machine learning model

170 Aerosol pH and $\epsilon(\text{NO}_3^-)$ exhibit nonlinear responses to multiple influencing factors. In this study, we employed a machine
 171 learning approach to investigate the effects of extreme dust storm conditions on aerosol pH and $\epsilon(\text{NO}_3^-)$. Specifically, we
 172 used the random forest (RF) algorithm to construct regression models tailored to aerosol pH and $\epsilon(\text{NO}_3^-)$ for each city
 173 under investigation. The dataset for the RF regression models was divided into a training set (80%) and a test set (20%).
 174 The training set was utilized to build the models, while the test set was used to validate their performance. The input
 175 predictive features for both aerosol pH and $\epsilon(\text{NO}_3^-)$ models included the water-soluble inorganic chemical composition
 176 of aerosols (Na^+ , SO_4^{2-} , NH_4^+ , NO_3^- , Cl^- , Ca^{2+} , K^+ , Mg^{2+}), gaseous species (NH_3 and HNO_3), and meteorological
 177 parameters (T and RH). To evaluate the model performance, we applied 5-fold cross-validation for parameter tuning.
 178 Model performance was evaluated using seven statistical metrics: Mean Absolute Error (MAE), Root Mean Squared Error
 179 (RMSE), Normalized Mean Squared Error (NMSE), Mean Bias (MB), Normalized Mean Bias (NMB), Index of
 180 Agreement (IOA), and the correlation coefficient (R). Detailed definitions and calculations for these metrics are provided
 181 in Supplementary Text 1. This machine learning based approach enabled us to quantify the complex, nonlinear
 182 relationships between aerosol properties, chemical compositions, and meteorological conditions, offering deeper insights
 183 into the drivers of aerosol pH and $\epsilon(\text{NO}_3^-)$ under varying dust pollution scenarios.

184 In addition, SHapley Additive exPlanations (SHAP), a method derived from the Shapley value concept in game theory,
 185 provides an interpretable framework to explain the predictions of complex machine learning models. SHAP quantifies
 186 the contribution of each input variable to individual predictions, making it a powerful tool for understanding model
 187 behavior (Duan et al., 2024; Lundberg and Lee, 2017). In this study, SHAP values were employed to assess the influence
 188 of various factors on aerosol pH and $\epsilon(\text{NO}_3^-)$ under dust storm and local dust conditions. A positive SHAP value for a
 189 given factor indicates that it contributes positively to the prediction, whereas a negative SHAP value implies a suppressive
 190 or inhibitory impact. This analysis allowed us to disentangle the relative contributions of chemical composition,
 191 meteorological conditions, and other variables to the variations in aerosol properties under different dust scenarios.



3. Results and Discussion

3.1 Observational evidence of anthropogenic and natural dust pollution

Dust emissions can be classified into anthropogenic and natural sources, with Ca^{2+} and Mg^{2+} commonly used as tracers. Figure 1 shows the relationship between the concentrations of Ca^{2+} and Mg^{2+} during the observation period from March to April 2023 across the three cities (Xuzhou, Zhenjiang, and Suzhou). It is evident that the concentrations of Ca^{2+} and Mg^{2+} exhibit two distinctly different linear slopes, indicating that the different dust origins during this period were influenced by both long-range transport dust storms and local dust emissions. In particular, during the period from April 11th to 13th, a severe dust storm originating was transmitted from northern regions, first impacting Hohhot, and then southward to the southern cities of the YRD region. As shown in Fig. 2a, the PM_{10} concentrations in the cities along the transport path exhibited a distinct gradient, with peak values reaching approximately $1702 \mu\text{g m}^{-3}$ in Hohhot, $1614 \mu\text{g m}^{-3}$ in Xuzhou, $925 \mu\text{g m}^{-3}$ in Zhenjiang, and $576 \mu\text{g m}^{-3}$ in Suzhou, respectively. In Xuzhou, the average concentration of Ca^{2+} increased from $0.47 \pm 0.36 \mu\text{g m}^{-3}$ during the local dust period to $2.00 \pm 1.66 \mu\text{g m}^{-3}$ during the dust storm period, marking a fourfold increase. Similarly, the average Ca^{2+} concentration rose from $0.30 \pm 0.23 \mu\text{g m}^{-3}$ to $1.69 \pm 1.41 \mu\text{g m}^{-3}$ in Zhenjiang, while the concentration increased from $0.35 \pm 0.26 \mu\text{g m}^{-3}$ to $0.92 \pm 0.52 \mu\text{g m}^{-3}$ in Suzhou.

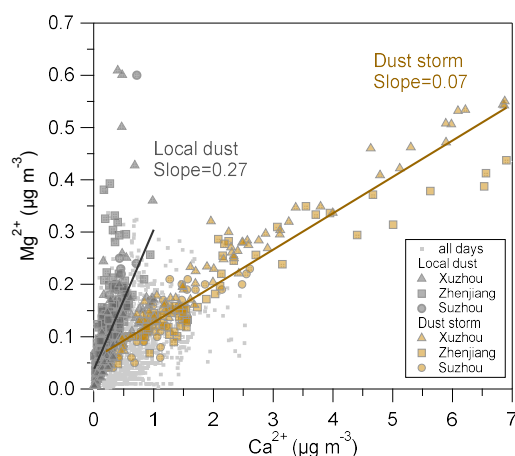
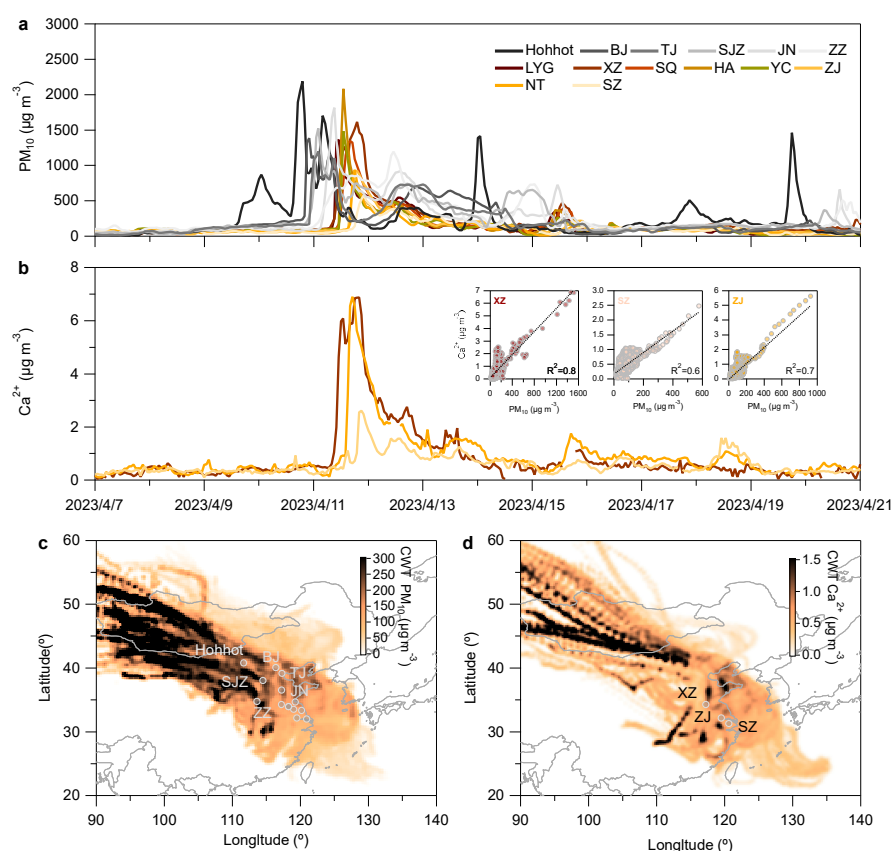


Figure 1. Relationship between Ca^{2+} and Mg^{2+} concentrations in $\text{PM}_{2.5}$ in Xuzhou (triangle), Zhenjiang (square), and Suzhou (circle). Dust types are distinguished based on the slope of the Ca^{2+} to Mg^{2+} concentration ratio, with local dust (gray) and dust storm (brown) indicated. Light gray dots represent the concentrations of Ca^{2+} and Mg^{2+} observed in the three cities during March – April 2023.

Figure 2a and b illustrate the temporal evolution of PM_{10} and Ca^{2+} concentrations during the dust storm, showing an initial



212 spike in Hohhot, followed by a gradual increase across the Beijing-Tianjin-Hebei (BTH) region, and eventual dispersion
 213 into several cities in Jiangsu Province. This progression is consistent with the CWT-weighted trajectory patterns shown
 214 in Fig. 2c and d, which delineate the transport pathways of the dust storm. The maps highlight significant contributions
 215 from Mongolia – the dust storm's origin – to regions including Hohhot, Beijing, Tianjin, Shijiazhuang, Jinan, Zhengzhou,
 216 and Jiangsu. This finding corroborates the results of Chen et al. (2023b), who attributed the dust storm to a strong cold
 217 high-pressure system and cold front that transported substantial quantities of coarse dust aerosols southward into the YRD
 218 region. Southward-moving cold fronts play a critical role in the diffusion and transport of atmospheric pollutants. In arid
 219 and semi-arid regions, these storms mobilize large amounts of crustal elements, such as Ca^{2+} , with high winds lifting dust
 220 from surface sources, including city streets, construction sites, and other exposed land areas (Ding et al., 2019).



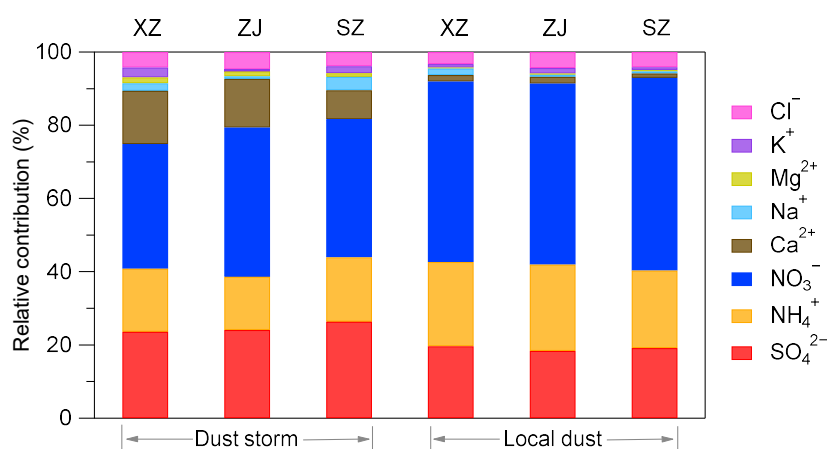
221
 222 **Figure 2.** Time series of PM₁₀ and Ca²⁺ concentrations, and their concentration-weighted trajectories for cities along the dust transport
 223 path. (a) Time series of PM₁₀ in 14 cities along the BTH region, and (b) Time series of Ca²⁺ concentrations in Xuzhou, Zhenjiang, and
 224 Suzhou and the correlation of Ca²⁺ and PM₁₀. (c) 48-hour CWT-weighted spatial distribution of PM₁₀ concentrations in 14 cities from



225 April 5 to 20, and (d) 48-hour CWT-weighted spatial distribution of Ca^{2+} concentrations in Xuzhou, Zhenjiang, and Suzhou (units: μg
 226 m^{-3}).

227

228 Figure 3 presents the relative contributions within $\text{PM}_{2.5}$ water-soluble inorganic species (WSIS) during local dust and
 229 dust storm periods in Xuzhou, Zhenjiang, and Suzhou. Across the three cities, the combined contribution of sulfate, nitrate,
 230 and ammonium consistently exceeded 80% of WSIS, confirming the importance of secondary inorganic aerosols in fine
 231 particulate pollution. Nitrate was the most significant contributor to WSIS during both periods, particularly during the
 232 local dust period, with an average contribution ranging from 49.3% to 52.6%. However, its relative contribution decreased
 233 during the dust storm period, dropping to 34.0% to 40.8%. In contrast, the relative contribution of sulfate increased during
 234 the dust storm period, with increments of 5.2%, 5.0%, and 6.7% in Xuzhou, Zhenjiang, and Suzhou, respectively. This
 235 suggests that the atmospheric dilution and dispersion effects during dust storms might impact nitrate aerosols more
 236 significantly than sulfate. The conclusion of Wang et al. (2022) also supports this result. Indeed, in eastern China, sulfate
 237 aerosols are more regionally distributed as secondary aerosol components, while nitrate formation is more influenced by
 238 local conditions (Wang et al., 2016; Zhang et al., 2015). As expected, during the dust storm period, the relative contribution
 239 of Ca^{2+} and Mg^{2+} increased across all three cities, with an average rise of approximately 10% compared to the local dust
 240 period..



241

242 **Figure 3.** Relative contributions of water-soluble inorganics (SO_4^{2-} , NH_4^+ , NO_3^- , Ca^{2+} , Na^+ , Mg^{2+} , K^+ , and Cl^-) within the $\text{PM}_{2.5}$ fraction
 243 in Xuzhou, Zhenjiang, and Suzhou during dust storm and local dust pollution periods, respectively.



244

245 **3.2 Driving factors of aerosol pH**

246 Aerosol pH plays a crucial role in influencing aerosol formation and chemical composition. By regulating the partitioning
 247 of semi-volatile compounds between the gas and particle phases, aerosol pH directly affects the distribution of particulate
 248 matter in the atmosphere (Guo et al., 2017b). To examine the factors influencing aerosol pH, we utilized the ISORROPIA-
 249 II thermodynamic model and sensitivity analysis to quantify the relative contributions of chemical and meteorological
 250 factors, such as T and RH, in Xuzhou, Zhenjiang, and Suzhou. The correlation between simulated and observed
 251 concentrations of NH_3 and particulate NO_3^- is presented in Fig. 4. Across all three cities, the simulated values exhibit
 252 strong agreement with measurements ($R^2 = 0.94 - 0.99$). Additionally, Fig. S2 shows high correlations ($R^2 = 0.90 - 0.97$)
 253 for particle-phase ammonium and chloride between ISORROPIA-II predictions and observations, confirming the robust
 254 performance of the thermodynamic model in this study.

255 To assess the impact of individual factors (TNO_3 , TNH_3 , Ca^{2+} , SO_4^{2-} , T and RH) on aerosol pH, we estimated their relative
 256 contributions using methods like those proposed by Zheng et al. (2020) and Zheng et al. (2022). First, we calculated the
 257 monthly average values for each factor in March and April, referred to as $pH_{i(3,3)}$ and $pH_{i(4,4)}$, respectively. Here, pH_i
 258 represents the influence of factor i on pH, with the numbers in parentheses indicating the respective months. For the
 259 analysis of a specific factor, we used the March average value of that factor while holding the other variables at their
 260 average levels for April. This yielded the aerosol pH value, denoted as $pH_{i(3,4)}$. Similarly, when using the April average
 261 value of the factor and maintaining the other variables at their March average levels, we recorded the resulting pH as
 262 $pH_{i(4,3)}$. The relative change in pH, denoted as $\Delta pH_{i(3)}$ and $\Delta pH_{i(4)}$ was calculated as the mean difference between
 263 $pH_{i(3,3)}$ and $pH_{i(4,3)}$, and between $pH_{i(4,4)}$ and $pH_{i(3,4)}$, respectively (see Eqs. 4 and 5). Finally, the overall impact of
 264 each factor on aerosol pH could be estimated (see Eq. 6).

$$265 \quad \Delta pH_{i(3)} = pH_{i(3,3)} - pH_{i(4,3)} \quad (4)$$

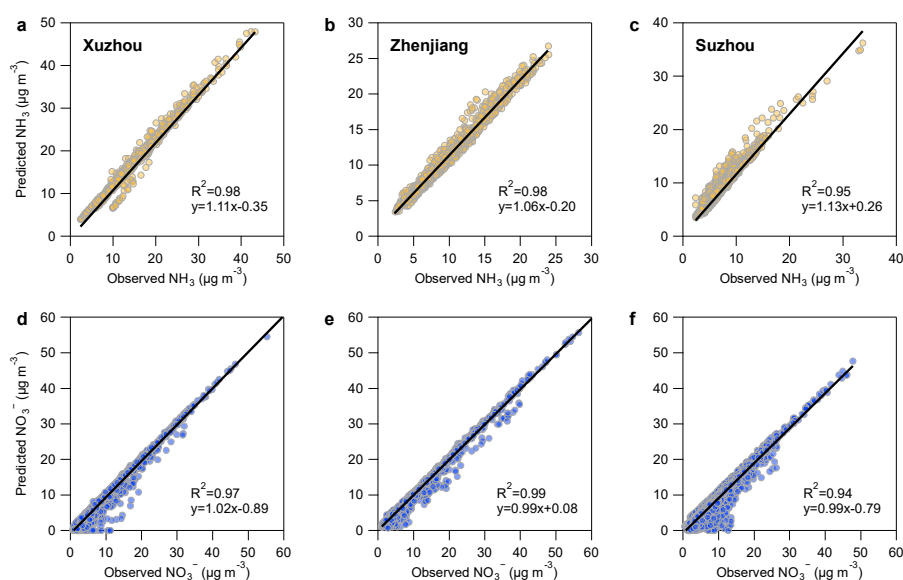
$$266 \quad \Delta pH_{i(4)} = pH_{i(4,4)} - pH_{i(3,4)} \quad (5)$$

$$267 \quad \Delta pH_i = \frac{[\Delta pH_{i(3)}] + [\Delta pH_{i(4)}]}{2} \quad (6)$$

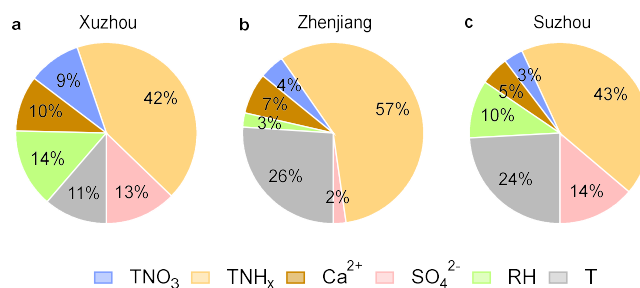
268 The impact of each factor could be positive or negative, which was detailed in Fig. S3. As shown in Fig. 5, atmospheric
 269 total ammonia emerged as the most significant driver of aerosol pH changes in all three cities, contributing 42%, 57%,



270 and 43% of the observed pH in Xuzhou, Zhenjiang, and Suzhou, respectively. Total ammonia led to ΔpH_{TNH_x} increases
 271 of 0.6, 1.3, and 0.5 units in these cities during spring 2023. For Zhenjiang, T and Ca^{2+} were the next most influential
 272 factors, contributing 0.6 and 0.15 units to ΔpH_T and $\Delta pH_{Ca^{2+}}$, respectively. Sulfate exhibited the smallest influence on
 273 aerosol pH, where a concentration change of $0.3 \mu g m^{-3}$ corresponded to a $\Delta pH_{SO_4^{2-}}$ of approximately 0.05 units. These
 274 results align with the findings of Weber et al. (2016), which suggest that aerosol pH is less sensitive to changes in sulfate
 275 concentrations compared to ammonia levels.



276 **Figure 4.** Correlation between ISORROPIA-II simulated and observed values of NH_3 and NO_3^- in three cities. (a) – (c) show the
 277 correlation between NH_3 predictions and observations, while (d) – (f) show the correlation between NO_3^- predictions and observations.
 278 The first column represents Xuzhou, the second column represents Zhenjiang, and the third column represents Suzhou.

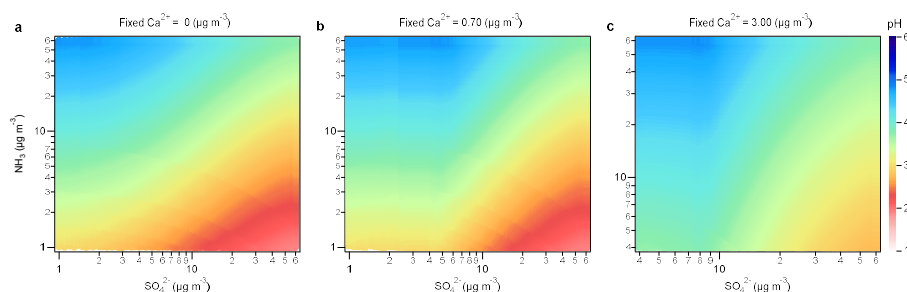


280 **Figure 5.** Relative contribution of different factors, including $TNO_3 = HNO_3 + NO_3^-$, $TNH_x = NH_3 + NH_4^+$, Ca^{2+} , SO_4^{2-} , RH, and T, to
 281 aerosol pH during the entire observation period in (a) Xuzhou, (b) Zhenjiang, and (c) Suzhou.
 282



283

284 To further explore the response of aerosol pH to variations in SO_4^{2-} and NH_3 concentrations under different dust conditions
 285 (non-dust, local dust, and extremely dust storm), we conducted sensitivity simulations constrained by observations from
 286 Zhenjiang as a case study. As illustrated in Fig. 6a – c, we extended the NH_3 and SO_4^{2-} concentration ranges beyond their
 287 observed values to encompass potential variations across the YRD region. The input concentrations of Na^+ , SO_4^{2-} , total
 288 chloride ($\text{TCl}_x = \text{Cl}^- + \text{HCl}$), K^+ , and Mg^{2+} were fixed at the average levels observed in Zhenjiang during the study period
 289 (see Table S2). Simulations were carried out under three distinct Ca^{2+} concentration scenarios: (1) non-dust ($\text{Ca}^{2+} = 0 \mu\text{g m}^{-3}$)
 290 m^{-3}), (2) local dust ($\text{Ca}^{2+} = 0.7 \mu\text{g m}^{-3}$), and (3) extremely dust storm ($\text{Ca}^{2+} = 3.00 \mu\text{g m}^{-3}$). In these simulations, total
 291 ammonia ($\text{TNH}_x = \text{NH}_4^+ + \text{NH}_3$) and total nitrate ($\text{TNO}_3 = \text{NO}_3^- + \text{HNO}_3$) concentrations were independently changed
 292 and input into the ISORROPIA-II model. Under non-dust conditions ($\text{Ca}^{2+} = 0 \mu\text{g m}^{-3}$), the model predicted lower aerosol
 293 pH values. As shown in Fig. 6a – b, a 5 – 10-fold increase in NH_3 concentration led to a pH increase of approximately 1
 294 unit, whereas aerosol pH demonstrated limited sensitivity to SO_4^{2-} concentration changes. This finding is consistent with
 295 previous studies (Zheng et al., 2022; Weber et al., 2016; Xie et al., 2020). However, under high Ca^{2+} concentration
 296 conditions, such as during extremely dust storm events, the influence of NH_3 on aerosol pH was notably mitigated (Fig.
 297 6c). The presence of Ca^{2+} during dust storms reduced the ability of NH_3 to modulate aerosol pH effectively. These results
 298 suggest that elevated Ca^{2+} concentrations, a characteristic of dust events, play a significant role in buffering the impact of
 299 NH_3 on aerosol pH.



300

301 **Figure 6.** Sensitivity of the pH to ammonia (NH_3) and sulfate (SO_4^{2-}) concentrations based on ISORROPIA-II model predictions under
 302 different Ca^{2+} concentration conditions: (a) 0, (b) 0.70, and (c) $3.00 \mu\text{g m}^{-3}$.

303

304 3.3 Impact of aerosol pH on the partitioning of nitric acid

305 In eastern China, nitrate has become a key component of $\text{PM}_{2.5}$, instead of sulfate (Xu et al., 2023; Gao et al., 2023). As



a semi-volatile compound, nitrate is strongly influenced by the gas-particle partitioning process in the atmosphere. Aerosol pH not only determines the stability of nitrate but also governs whether it exists in the particulate phase or volatilizes as HNO_3 in the gas phase (Guo et al., 2018). At higher pH, nitrate tends to exist in the particle phase due to the oxidation of NO_x , while under lower pH conditions, nitrate is more likely to volatilize into the gas phase as HNO_3 (Nenes et al., 2020). Using Eq. (2), we analyzed the relationship between the nitrate particle-phase fraction ($\varepsilon(\text{NO}_3^-)$) and aerosol pH for three cities – Xuzhou, Zhenjiang, and Suzhou – under dust storm and local dust conditions. Fig. 7 shows the S-shaped curve representing this relationship, calculated based on the average T and aerosol W_i during dust storm and local dust conditions, assuming ideal solution behavior (activity coefficient $\gamma_{H^+} = 1$). This curve visually demonstrates the regulation of nitrate phase partitioning by aerosol pH under these conditions and provides a theoretical basis for controlling the effect of ammonia on particulate nitrate formation by adjusting aerosol pH (Guo et al., 2018).

As cities along the dust storm transport path, Xuzhou, Zhenjiang, and Suzhou experience varying degrees of dust influence, leading to significant differences in aerosol pH. On average, aerosol pH is elevated during dust storms compared to local dust conditions. During dust storms, the mean aerosol pH values were 5.50 ± 1.65 in Xuzhou, 5.44 ± 1.69 in Zhenjiang, and 5.30 ± 1.67 in Suzhou. Under local dust conditions, these values were lower, at 4.12 ± 0.52 , 3.92 ± 0.32 , and 3.74 ± 0.69 respectively. Xuzhou, situated at the northern edge of the dust storm transport path, exhibited the highest aerosol pH during both periods, reflecting the substantial impact of transported dust pollution. The S-shaped curve in Fig. 7 demonstrates that under both dust storm and local dust conditions, the average aerosol pH aligns with nitrate particle-phase fractions exceeding 99%, indicating that nitrate predominantly resides in the particle phase. This finding highlights the promoting effect of dust pollution on the gas-to-particle transformation of nitrate.

When aerosol pH drops below 3, however, $\varepsilon(\text{NO}_3^-)$ decreases sharply, signifying the onset of nitrate volatilization into the gas phase. Notably, when aerosol pH lies in the range of 1 to 3, $\varepsilon(\text{NO}_3^-)$ exhibits heightened sensitivity to aerosol pH changes. This trend was consistently observed across all three cities. Reducing NH_3 concentrations is particularly effective in influencing nitrate gas-particle partitioning when aerosol pH is within this sensitive range, offering a promising strategy to mitigate regional particulate nitrate pollution. However, environments with dust pollution may disrupt this theoretical relationship. NVCs (such as Ca^{2+}) in dust can neutralize acidic aerosol components, maintaining aerosol pH at relatively high levels (e.g., $\text{pH} > \text{approximately } 3.5$) (Fig. 7). This neutralization effect limits the ability to lower particulate nitrate concentrations solely by reducing NH_3 emissions, necessitating alternative approaches to address nitrate-driven air quality challenges in dust-influenced regions.

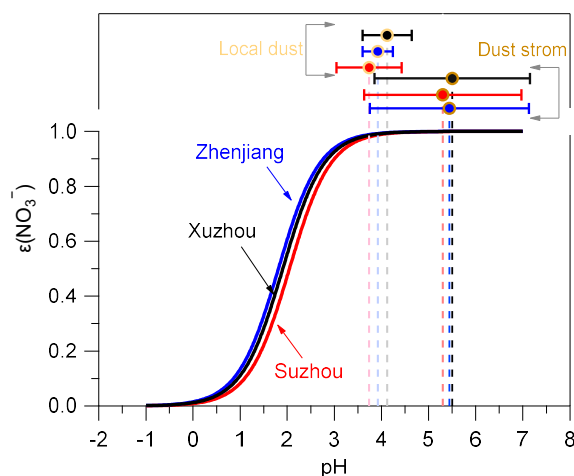


Figure 7. S-curve distributions for $\varepsilon(\text{NO}_3^-)$ under the conditions from different cities. Based on Eq. (2), the relationship between $\varepsilon(\text{NO}_3^-)$ and pH was calculated using the average T and W_i during dust storm and local dust periods (assuming $\gamma_{\text{NO}_3^-}\gamma_{\text{H}^+}=0.28$, $\gamma_{\text{H}^+}=1$). The vertical dashed lines represent the average pH values calculated using ISORROPIA-II for the three cities. Error bars indicate the sample standard deviation of aerosol pH.

To further quantify the impact of dust storms on aerosol pH and $\varepsilon(\text{NO}_3^-)$, we utilized the RF model combined with SHAP values for both prediction and sensitivity analysis. The correlation between the observed and predicted results from the RF model is shown in Fig. S4. The Index of Agreement (IOA) values ranged from 0.93 to 0.97, indicating a high level of model agreement. Meanwhile, the correlation coefficients (R) varied between 0.78 and 0.90, further validating the model's predictive accuracy. For aerosol pH predictions, five evaluation metrics were used: MAE, RMSE, NMSE, MB, and NMB. The values for MAE ranged from 0.13 to 0.18, while RMSE values were between 0.26 and 0.29. For NMSE, the values ranged from 0.10 to 0.12, and the biases (MB and NMB) varied from -0.01 to -0.006 and 0.004 to 0.007, respectively. In comparison, the corresponding evaluation metrics for $\varepsilon(\text{NO}_3^-)$ were as follows: MAE ranged from 0.01 to 0.02, RMSE from 0.03 to 0.04, and NMSE from 0.10 to 0.21. The bias values for $\varepsilon(\text{NO}_3^-)$ ranged from -0.00006 to 0.004 for MB and from 0.003 to 0.007 for NMB. These statistical results demonstrate the reliability and robustness of the RF model in predicting aerosol pH and nitrate partitioning.

Figure 8 illustrates the impact of dust storms and local dust conditions on aerosol pH and $\varepsilon(\text{NO}_3^-)$. The ΔSHAP values represent the difference between the average SHAP values of all variables during dust storm periods and the average SHAP values for all variables during the non-dust storm period. During dust storm conditions, ΔSHAP significantly increased in Xuzhou, Zhenjiang, and Suzhou, with aerosol pH values rising by $\Delta 1.2$, $\Delta 1.5$, and $\Delta 1.5$ units, respectively



(Fig. 8 a-c). This result is consistent with our previous conclusion that dust storms contribute to an increase in aerosol pH, confirming the positive impact of dust storms on the random forest model's predictions of aerosol pH. Similarly, Fig. 8 d-f shows the changes in $\epsilon(\text{NO}_3^-)$ for the three cities under different weather conditions. It is evident that the effect of dust storms on $\epsilon(\text{NO}_3^-)$ is 10 to 20 times greater than the impact of local non-dust storm conditions. This indicates that dust storm conditions have a significantly stronger positive contribution to the particle-phase fraction of nitrate. The presence of dust particles facilitates the conversion of nitrate to the particulate phase, highlighting the significant influence of dust storms on nitrate partitioning in the atmosphere.

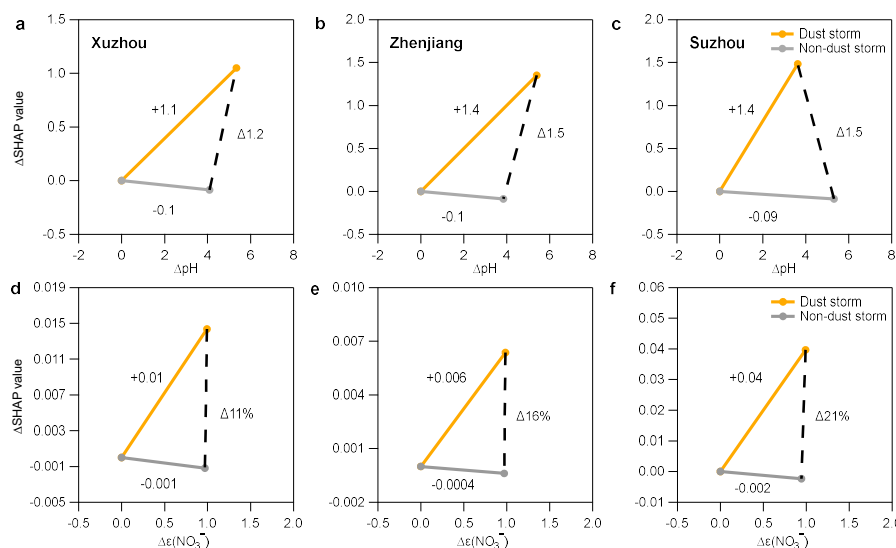


Figure 8. ΔSHAP values for (a) – (c) aerosol pH and (d) – (f) $\epsilon(\text{NO}_3^-)$. The orange solid line represents the impact of dust storms, the gray solid line represents the non-dust scenario, and the black dashed line shows the difference between the two scenarios.

3.4 Effectiveness of emission reduction on particulate nitrate under dust pollution

To explore the impact of emission reductions of TNH_x , TNO_3 , and SO_4^{2-} on $\epsilon(\text{NO}_3^-)$ during different dust storm conditions, we conducted a sensitivity analysis using the average pollutant concentrations observed in Zhenjiang during the spring of 2023. The results, shown in Fig. 9, demonstrate a nonlinear response of both $\epsilon(\text{NO}_3^-)$ and the total ammonium-nitrate concentration ($\text{NH}_4^+ + \text{NO}_3^-$) to reductions in TNH_x , TNO_3 , and SO_4^{2-} , respectively. We simulated the effects of progressively reducing TNH_x , TNO_3 , and SO_4^{2-} by 0% to 50% under different Ca^{2+} concentration conditions, which include different dust pollution scenarios. For the simulation, Ca^{2+} concentration was set to $0.1 \mu\text{g m}^{-3}$ for local dust



conditions and ranged from 0.7 to 3.0 $\mu\text{g m}^{-3}$ for dust storm conditions. When the Ca^{2+} concentration exceeded 3 $\mu\text{g m}^{-3}$, further reductions in the other variables had negligible effects on the output, with emission reductions having little to no impact on $\epsilon(\text{NO}_3^-)$.

As shown in Fig. 9a, it is evident that during local dust conditions, $\epsilon(\text{NO}_3^-)$ remained relatively constant until TNH_x emissions were reduced by 30%. At this point, $\epsilon(\text{NO}_3^-)$ rapidly dropped from 99%, signaling the onset of a significant shift in the gas-particle partitioning of nitrate. When TNH_x reductions reached 50%, $\epsilon(\text{NO}_3^-)$ fell sharply to approximately 30%, indicating that nitrate transitioned predominantly into its gas-phase form. This simulation result is consistent with the sensitivity analysis of NH_3 concentrations in section 3.2, which also showed a significant response in nitrate partitioning as NH_3 concentrations decreased. Thus, in the Zhenjiang region, a 30% reduction in TNH_x emissions is necessary to effectively reduce the mass of $(\text{NH}_4^+ + \text{NO}_3^-)$ during spring (Fig. 10 d). In contrast, during dust storm conditions (Fig. 9a), the reduction in TNH_x had a much more subdued effect on $\epsilon(\text{NO}_3^-)$, especially at higher Ca^{2+} concentrations (above 2.5 $\mu\text{g m}^{-3}$), where the reduction had almost no impact on $\epsilon(\text{NO}_3^-)$.

For TNO_3 reductions, as shown in Fig. 10 b, the changes in $\epsilon(\text{NO}_3^-)$ were minimal, regardless of the Ca^{2+} concentration. However, during local dust conditions (Fig. 9e), the reduction of TNO_3 led to a significant decrease in $(\text{NH}_4^+ + \text{NO}_3^-)$ concentrations, indicating that TNO_3 reduction was particularly effective under local dust conditions. Lastly, reductions in SO_4^{2-} emissions (Fig. 9c and f) had a smaller impact on both $\epsilon(\text{NO}_3^-)$ and $(\text{NH}_4^+ + \text{NO}_3^-)$ concentrations. Interestingly, at very low dust concentrations, SO_4^{2-} reductions could even lead to a slight increase (by up to 0.5%) in $\epsilon(\text{NO}_3^-)$, indicating that sulfate reduction alone is not an effective strategy for controlling nitrate partitioning.

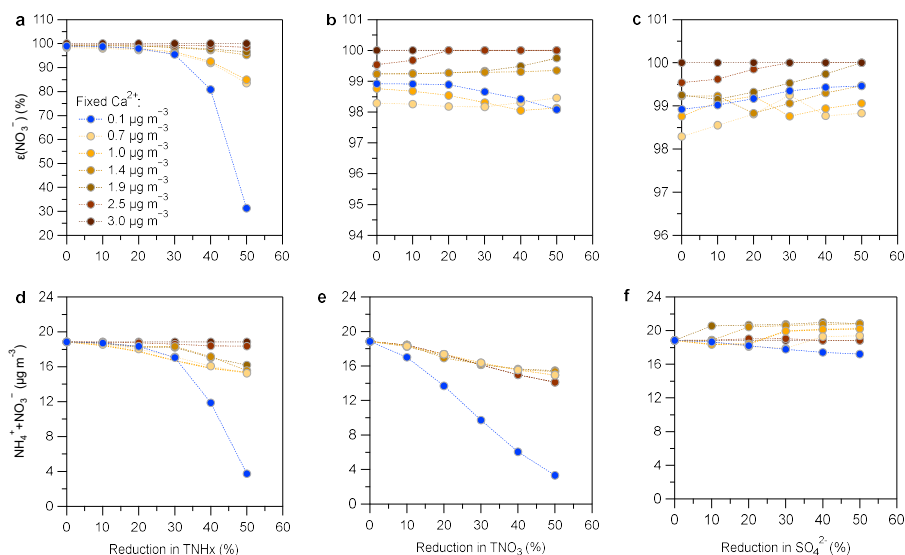


Figure 9. Sensitivity analysis simulating the impact of reducing TNH_x ($\text{TNH}_x = \text{NH}_3 + \text{NH}_4^+$), TNO_3 ($\text{TNO}_3 = \text{HNO}_3 + \text{NO}_3^-$), and SO_4^{2-} by 0-50% during dust events of varying intensities on $\epsilon(\text{NO}_3^-)$ and $\text{NH}_4^+ + \text{NO}_3^-$.

4. Conclusions and Impactions

This study explores the impact of dust pollution on aerosol pH and nitrate gas-particle partitioning in three cities across the YRD region of Eastern China. By combining field observations, thermodynamic modeling, and machine learning techniques, we provide a comprehensive analysis of how different dust scenarios affect urban aerosol pH and gas-particle partitioning chemistry of nitrate. Our analysis of a dust storm event that originated in Mongolia and was transported over long distances to the YRD region in the spring of 2023 revealed a significant increase in PM_{10} concentrations, the average PM_{10} concentration in three cities along the route exceeds $400 \mu\text{g m}^{-3}$, approximately four times higher than during local dust events. Thermodynamic simulations using the ISORROPIA model showed that both ammonia and calcium ion concentrations strongly influenced aerosol pH, with average contributions of 47% and 7% respectively. Random forest model simulations further indicated that the presence of high NVCs during dust storms significantly contributed to changes in aerosol pH (1.2 – 1.5 units). Sensitivity analysis of pH responses to sulfate and NH_3 concentrations under different dust conditions (non-dust, local dust, and extremely dust storm) revealed that a 5 to 10 fold increase in NH_3 led to a 1-unit change in aerosol pH. Machine learning analysis showed that extreme dust storm events contributed



408 approximately 1.4 units to the increase in aerosol pH, with a corresponding increase in nitrate partitioning (16%). This
409 suggests that under high aerosol pH conditions during dust pollution periods, nitrate is predominantly in the particulate
410 phase, indicating that dust significantly inhibits the partitioning of nitrate into the gaseous phase. In addition, our
411 sensitivity analyses also showed that ammonia reduction had the most significant effect on reducing nitrate aerosols under
412 dust-free conditions. However, the effectiveness of ammonia reductions in lowering nitrate aerosol concentrations was
413 significantly reduced due to the influence of NVCs on nitrate partitioning under dust pollution scenarios. These findings
414 suggest that dust pollution can substantially weaken the impact of ammonia reductions on nitrate aerosol formation,
415 highlighting the need for targeted control strategies during dust storm events. Dust emission remains a significant air
416 pollution concern worldwide, while urban nitrate aerosol pollution is a pressing issue in many cities, particularly in East
417 Asia, where the frequency of natural dust events has increased in recent years. These dust storms, along with
418 anthropogenic dust, can substantially alter aerosol chemistry by modifying aerosol pH and nitrate partitioning. Therefore,
419 effective dust control strategies are critical for mitigating the adverse effects of aerosol acidity on nitrate aerosol formation
420 and improving air quality in dust-prone regions.

421



422 *Data availability.* Additional meteorological parameters can be accessed at the European Centre for Medium-Range
 423 Weather Forecasts (ECMWF) ERA5 reanalysis dataset (<https://cds.climate.copernicus.eu/>; last access: 21 November
 424 2023). Reginal PM₁₀ data can be accessed at the China National Environmental Monitoring Centre
 425 (<https://air.cnemc.cn:18007/>; 21 last access: November, 2023). The additional data will be made available upon request
 426 (yjzhang@nuist.edu.cn).

428 *Author contributions.*

429 YZ conceived and designed the study. HL and YZ conducted the simulations and data analysis. HL, YZ, SZ, YR, JQ,
 430 and MZ carried out field measurements and validated the data. HL and YZ wrote the original manuscript, while DL, FC,
 431 OF, HD, and XG provided critical feedback and contributed to the manuscript revisions.

433 *Competing interests.* The authors declare that they have no conflict of interest.

435 *Acknowledgements.*

436 This study was supported by the National Natural Science Foundation of China (grant no. 42207124) and Natural
 437 Science Foundation of Jiangsu Province (grant no. BK20210663).

438 **References**

- 439 Beaudor, M., Hauglustaine, D., Lathière, J., Van Damme, M., Clarisse, L., and Vuichard, N.: Evaluating present-day and
 440 future impacts of agricultural ammonia emissions on atmospheric chemistry and climate, EGU sphere, 2024, 1–40,
 441 <https://doi.org/10.5194/egusphere-2024-2022>, 2024.
- 442 Boichu, M., Favez, O., Riffault, V., Petit, J. E., Zhang, Y., Brogniez, C., Sciare, J., Chiapello, I., Clarisse, L., Zhang, S.,
 443 Pujol-Söhne, N., Tison, E., Delbarre, H., and Goloub, P.: Large-scale particulate air pollution and chemical fingerprint
 444 of volcanic sulfate aerosols from the 2014–2015 Holuhraun flood lava eruption of Bárðarbunga volcano (Iceland),
 445 Atmos. Chem. Phys., 19, 14253–14287, <https://doi.org/10.5194/acp-19-14253-2019>, 2019.
- 446 Chen, S., Chen, J., Zhang, Y., Lin, J., Bi, H., Song, H., Chen, Y., Lian, L., Liu, C., and Zhang, R.: Anthropogenic dust:
 447 sources, characteristics and emissions, Environ. Res. Lett., 18, 103002, <https://doi.org/10.1088/1748-9326/acf479>,
 448 2023a.



- 449 Chen, S., Zhao, D., Huang, J., He, J., Chen, Y., Chen, J., Bi, H., Lou, G., Du, S., Zhang, Y., and Yang, F.: Mongolia
 450 Contributed More than 42% of the Dust Concentrations in Northern China in March and April 2023, *Adv. Atmos. Sci.*,
 451 40, 1549-1557, <https://doi.org/10.1007/s00376-023-3062-1>, 2023b.
- 452 Chen, S., Jiang, N., Huang, J., Xu, X., Zhang, H., Zang, Z., Huang, K., Xu, X., Wei, Y., Guan, X., Zhang, X., Luo, Y., Hu,
 453 Z., and Feng, T.: Quantifying contributions of natural and anthropogenic dust emission from different climatic regions,
 454 *Atmos. Environ.*, 191, 94-104, <https://doi.org/10.1016/j.atmosenv.2018.07.043>, 2018.
- 455 Chen, Y., Chen, S., Zhou, J., Zhao, D., Bi, H., Zhang, Y., Alam, K., Yu, H., Yang, Y., and Chen, J.: A super dust storm
 456 enhanced by radiative feedback, *npj Clim. Atmos. Sci.*, 6, 90, <https://doi.org/10.1038/s41612-023-00418-y>, 2023c.
- 457 Clegg, S. L., Brimblecombe, P., and Wexler, A. S.: Thermodynamic Model of the System $\text{H}^+ - \text{NH}_4^+ - \text{SO}_4^{2-} - \text{NO}_3^- - \text{H}_2\text{O}$
 458 at Tropospheric Temperatures, *J. Phys. Chem. A*, 102, 2137-2154, <https://doi.org/10.1021/jp973042r>, 1998.
- 459 Ding, J., Zhao, P., Su, J., Dong, Q., Du, X., and Zhang, Y.: Aerosol pH and its driving factors in Beijing, *Atmos. Chem.*
 460 *Phys.*, 19, 7939-7954, <https://doi.org/10.5194/acp-19-7939-2019>, 2019.
- 461 Duan, J., Huang, R.-J., Wang, Y., Xu, W., Zhong, H., Lin, C., Huang, W., Gu, Y., Ovadnevaite, J., Ceburnis, D., and
 462 O'Dowd, C.: Measurement report: Size-resolved secondary organic aerosol formation modulated by aerosol water
 463 uptake in wintertime haze, *Atmos. Chem. Phys.*, 24, 7687-7698, <https://doi.org/10.5194/acp-24-7687-2024>, 2024.
- 464 Fang, T., Guo, H., Zeng, L., Verma, V., Nenes, A., and Weber, R. J.: Highly Acidic Ambient Particles, Soluble Metals, and
 465 Oxidative Potential: A Link between Sulfate and Aerosol Toxicity, *Environ. Sci. Technol.*, 51, 2611-2620,
 466 <https://doi.org/10.1021/acs.est.6b06151>, 2017.
- 467 Fountoukis, C. and Nenes, A.: ISORROPIA II: a computationally efficient thermodynamic equilibrium model for K^+ -
 468 Ca^{2+} - Mg^{2+} - NH_4^+ - Na^+ - SO_4^{2-} - NO_3^- - Cl^- - H_2O aerosols, *Atmos. Chem. Phys.*, 7, 4639-4659,
 469 <https://doi.org/10.5194/acp-7-4639-2007>, 2007.
- 470 Fu, X., Wang, S. X., Cheng, Z., Xing, J., Zhao, B., Wang, J. D., and Hao, J. M.: Source, transport and impacts of a heavy
 471 dust event in the Yangtze River Delta, China, in 2011, *Atmos. Chem. Phys.*, 14, 1239-1254, [https://doi.org/10.5194/acp-](https://doi.org/10.5194/acp-14-1239-2014)
 472 [14-1239-2014](https://doi.org/10.5194/acp-14-1239-2014), 2014.
- 473 Gao, D., Zhao, B., Wang, S., Wang, Y., Gaudet, B., Zhu, Y., Wang, X., Shen, J., Li, S., He, Y., Yin, D., and Dong, Z.:
 474 Increased importance of aerosol-cloud interactions for surface $\text{PM}_{2.5}$ pollution relative to aerosol-radiation
 475 interactions in China with the anthropogenic emission reductions, *Atmos. Chem. Phys.*, 23, 14359-14373,
 476 <https://doi.org/10.5194/acp-23-14359-2023>, 2023.



- 477 Geng, G., Zhang, Q., Tong, D., Li, M., Zheng, Y., Wang, S., and He, K.: Chemical composition of ambient PM_{2.5} over
 478 China and relationship to precursor emissions during 2005–2012, *Atmos. Chem. Phys.*, 17, 9187–9203,
 479 <https://doi.org/10.5194/acp-17-9187-2017>, 2017.
- 480 Goudie, A. S.: Desert dust and human health disorders, *Environ. Int.*, 63, 101–113,
 481 <https://doi.org/10.1016/j.envint.2013.10.011>, 2014.
- 482 Guo, H., Weber, R. J., and Nenes, A.: High levels of ammonia do not raise fine particle pH sufficiently to yield nitrogen
 483 oxide-dominated sulfate production, *Sci. Rep.*, 7, 12109, <https://doi.org/10.1038/s41598-017-11704-0>, 2017a.
- 484 Guo, H., Otjes, R., Schlag, P., Kiendler-Scharr, A., Nenes, A., and Weber, R. J.: Effectiveness of ammonia reduction on
 485 control of fine particle nitrate, *Atmos. Chem. Phys.*, 18, 12241–12256, <https://doi.org/10.5194/acp-18-12241-2018>,
 486 2018.
- 487 Guo, H., Liu, J., Froyd, K. D., Roberts, J. M., Veres, P. R., Hayes, P. L., Jimenez, J. L., Nenes, A., and Weber, R. J.: Fine
 488 particle pH and gas–particle phase partitioning of inorganic species in Pasadena, California, during the 2010 CalNex
 489 campaign, *Atmos. Chem. Phys.*, 17, 5703–5719, <https://doi.org/10.5194/acp-17-5703-2017>, 2017b.
- 490 Guo, H., Sullivan, A. P., Campuzano-Jost, P., Schroder, J. C., Lopez-Hilfiker, F. D., Dibb, J. E., Jimenez, J. L., Thornton,
 491 J. A., Brown, S. S., Nenes, A., and Weber, R. J.: Fine particle pH and the partitioning of nitric acid during winter in the
 492 northeastern United States, *J. Geophys. Res. Atmos.*, 121, 10,355 – 310,376, <https://doi.org/10.1002/2016JD025311>,
 493 2016.
- 494 Guo, H., Xu, L., Bougiatioti, A., Cerully, K. M., Capps, S. L., Hite, J. R., Carlton, A. G., Lee, S. H., Bergin, M. H., Ng,
 495 N. L., Nenes, A., and Weber, R. J.: Fine-particle water and pH in the southeastern United States, *Atmos. Chem. Phys.*,
 496 15, 5211–5228, <https://doi.org/10.5194/acp-15-5211-2015>, 2015.
- 497 Hauglustaine, D. A., Balkanski, Y., and Schulz, M.: A global model simulation of present and future nitrate aerosols and
 498 their direct radiative forcing of climate, *Atmos. Chem. Phys.*, 14, 11031–11063, [https://doi.org/10.5194/acp-14-11031-](https://doi.org/10.5194/acp-14-11031-2014)
 499 [2014](https://doi.org/10.5194/acp-14-11031-2014), 2014.
- 500 Hrdina, A., Murphy, J. G., Hallar, A. G., Lin, J. C., Moravek, A., Bares, R., Petersen, R. C., Franchin, A., Middlebrook,
 501 A. M., Goldberger, L., Lee, B. H., Baasandorj, M., and Brown, S. S.: The role of coarse aerosol particles as a sink of
 502 HNO₃ in wintertime pollution events in the Salt Lake Valley, *Atmos. Chem. Phys.*, 21, 8111–
 503 8126, <https://doi.org/10.5194/acp-21-8111-2021>, 2021.
- 504 Huang, J., Fu, Q., Zhang, W., Wang, X., Zhang, R., Ye, H., and Warren, S. G.: Dust and Black Carbon in Seasonal Snow



- 505 Across Northern China, *Bull. Am. Meteorol.*, 92, 175-181, <https://doi.org/10.1175/2010BAMS3064.1>, 2011.
- 506 Jickells, T. D., An, Z. S., Andersen, K. K., Baker, A. R., Bergametti, G., Brooks, N., Cao, J. J., Boyd, P. W., Duce, R. A.,
 507 Hunter, K. A., Kawahata, H., Kubilay, N., laRoche, J., Liss, P. S., Mahowald, N., Prospero, J. M., Ridgwell, A. J., Tegen,
 508 I., and Torres, R.: Global Iron Connections Between Desert Dust, Ocean Biogeochemistry, and Climate, *Science*, 308,
 509 67-71, <https://doi.org/10.1126/science.1105959>, 2005.
- 510 Kurokawa, J. and Ohara, T.: Long-term historical trends in air pollutant emissions in Asia: Regional Emission inventory
 511 in ASIA (REAS) version 3, *Atmos. Chem. Phys.*, 20, 12761-12793, 10.5194/acp-20-12761-2020, 2020.
- 512 Li, J., Zhang, N., Tian, P., Zhang, M., Shi, J., Chang, Y., Zhang, L., Liu, Z., and Wang, Y.: Significant roles of aged dust
 513 aerosols on rapid nitrate formation under dry conditions in a semi-arid city, *Environmental Pollution*, 336, 122395,
 514 <https://doi.org/10.1016/j.envpol.2023.122395>, 2023.
- 515 Liu, X., Song, H., Lei, T., Liu, P., Xu, C., Wang, D., Yang, Z., Xia, H., Wang, T., and Zhao, H.: Effects of natural and
 516 anthropogenic factors and their interactions on dust events in Northern China, *Catena*, 196, 104919,
 517 <https://doi.org/10.1016/j.catena.2020.104919>, 2021.
- 518 Liu, Y., Zhan, J., Zheng, F., Song, B., Zhang, Y., Ma, W., Hua, C., Xie, J., Bao, X., Yan, C., Bianchi, F., Petäjä, T., Ding,
 519 A., Song, Y., He, H., and Kulmala, M.: Dust emission reduction enhanced gas-to-particle conversion of ammonia in
 520 the North China Plain, *Nat. Commun.*, 13, 6887, <https://doi.org/10.1038/s41467-022-34733-4>, 2022.
- 521 Lundberg, S. M. and Lee, S.-I.: A unified approach to interpreting model predictions, *Proceedings of the 31st International*
 522 *Conference on Neural Information Processing Systems*, Long Beach, California, USA,
 523 <https://doi.org/10.48550/arXiv.1705.07874>, 2017.
- 524 Mahowald, N. M., Muhs, D. R., Levis, S., Rasch, P. J., Yoshioka, M., Zender, C. S., and Luo, C.: Change in atmospheric
 525 mineral aerosols in response to climate: Last glacial period, preindustrial, modern, and doubled carbon dioxide climates,
 526 *J. Geophys. Res. Atmos.*, 111, <https://doi.org/10.1029/2005JD006653>, 2006.
- 527 Malm, W. C. and Day, D. E.: Estimates of aerosol species scattering characteristics as a function of relative humidity,
 528 *Atmospheric Environment*, 35, 2845-2860, [https://doi.org/10.1016/S1352-2310\(01\)00077-2](https://doi.org/10.1016/S1352-2310(01)00077-2), 2001.
- 529 Metzger, S., Dentener, F., Pandis, S., and Lelieveld, J.: Gas/aerosol partitioning: 1. A computationally efficient model, *J.*
 530 *Geophys. Res. Atmos.*, 107, <https://doi.org/10.1029/2001JD001102>, 2002.
- 531 Milousis, A., Klingmüller, K., Tsimpidi, A. P., Kok, J. F., Kanakidou, M., Nenes, A., and Karydis, V. A.: Impact of mineral
 532 dust on the global nitrate aerosol direct and indirect radiative effect, *Atmos. Chem. Phys.*, 1579,



- 533 <https://doi.org/10.5194/egusphere-2024-1579>, 2024.
- 534 Nah, T., Guo, H., Sullivan, A. P., Chen, Y., Tanner, D. J., Nenes, A., Russell, A., Ng, N. L., Huey, L. G., and Weber, R. J.:
 535 Characterization of aerosol composition, aerosol acidity, and organic acid partitioning at an agriculturally intensive
 536 rural southeastern US site, *Atmos. Chem. Phys.*, 18, 11471-11491, <https://doi.org/10.5194/acp-18-11471-2018>, 2018.
- 537 Nenes, A., Pandis, S. N., Weber, R. J., and Russell, A.: Aerosol pH and liquid water content determine when particulate
 538 matter is sensitive to ammonia and nitrate availability, *Atmos. Chem. Phys.*, 20, 3249-3258,
 539 <https://doi.org/10.5194/acp-20-3249-2020>, 2020.
- 540 Nenes, A., Pandis, S. N., Kanakidou, M., Russell, A. G., Song, S., Vasilakos, P., and Weber, R. J.: Aerosol acidity and
 541 liquid water content regulate the dry deposition of inorganic reactive nitrogen, *Atmos. Chem. Phys.*, 21, 6023-6033,
 542 <https://doi.org/10.5194/acp-21-6023-2021>, 2021.
- 543 Nguyen, T. B., Coggon, M. M., Bates, K. H., Zhang, X., Schwantes, R. H., Schilling, K. A., Loza, C. L., Flagan, R. C.,
 544 Wennberg, P. O., and Seinfeld, J. H.: Organic aerosol formation from the reactive uptake of isoprene epoxydiols
 545 (IEPOX) onto non-acidified inorganic seeds, *Atmos. Chem. Phys.*, 14, 3497-3510, [https://doi.org/10.5194/acp-14-](https://doi.org/10.5194/acp-14-3497-2014)
 546 [3497-2014](https://doi.org/10.5194/acp-14-3497-2014), 2014.
- 547 Notaro, M., Yu, Y., and Kalashnikova, O. V.: Regime shift in Arabian dust activity, triggered by persistent Fertile Crescent
 548 drought, *J. Geophys. Res. Atmos.*, 120, 10,229-210,249, <https://doi.org/10.1002/2015JD023855>, 2015.
- 549 Petit, J.-E., Favez, O., Albinet, A., and Canonaco, F.: A user-friendly tool for comprehensive evaluation of the
 550 geographical origins of atmospheric pollution: Wind and trajectory analyses, *Environ. Model. Softw.*, 88, 183-187,
 551 <https://doi.org/10.1016/j.envsoft.2016.11.022>, 2017.
- 552 Rosenfeld, D., Rudich, Y., and Lahav, R.: Desert dust suppressing precipitation: A possible desertification feedback loop,
 553 *Proc. Natl. Acad. Sci. U.S.A.*, 98, 5975-5980, <https://doi.org/10.1073/pnas.101122798>, 2001.
- 554 Rumsey, I. C., Cowen, K. A., Walker, J. T., Kelly, T. J., Hanft, E. A., Mishoe, K., Rogers, C., Proost, R., Beachley, G. M.,
 555 Lear, G., Frelink, T., and Otjes, R. P.: An assessment of the performance of the Monitor for AeRosols and GAsEs in
 556 ambient air (MARGA): a semi-continuous method for soluble compounds, *Atmos. Chem. Phys.*, 14, 5639-5658,
 557 <https://doi.org/10.5194/acp-14-5639-2014>, 2014.
- 558 Schaap, M., Spindler, G., Schulz, M., Acker, K., Maenhaut, W., Berner, A., Wieprecht, W., Streit, N., Müller, K.,
 559 Brüggemann, E., Chi, X., Putaud, J. P., Hitznerberger, R., Puxbaum, H., Baltensperger, U., and ten Brink, H.: Artefacts
 560 in the sampling of nitrate studied in the “INTERCOMP” campaigns of EUROTRAC-AEROSOL, *Atmos. Environ.*, 38,



- 561 6487-6496, <https://doi.org/10.1016/j.atmosenv.2004.08.026>, 2004.
- 562 Seinfeld, J. H., Pandis, S. N., and Noone, K. J.: Atmospheric Chemistry and Physics: From Air Pollution to Climate
563 Change, *Physics Today*, 51, 88-90, <https://www.wiley.com/en-cn/9781118947401>, 1998.
- 564 Shao, Y. and Dong, C. H.: A review on East Asian dust storm climate, modelling and monitoring, *Glob. Planet. Change*,
565 52, 1-22, <https://doi.org/10.1016/j.gloplacha.2006.02.011>, 2006.
- 566 Shi, X., Nenes, A., Xiao, Z., Song, S., Yu, H., Shi, G., Zhao, Q., Chen, K., Feng, Y., and Russell, A. G.: High-Resolution
567 Data Sets Unravel the Effects of Sources and Meteorological Conditions on Nitrate and Its Gas-Particle Partitioning,
568 *Environ. Sci. Technol.*, 53, 3048-3057, <https://doi.org/10.1021/acs.est.8b06524>, 2019.
- 569 Song, C. H., Carmichael, G.R.: Gas-Particle Partitioning of Nitric Acid Modulated by Alkaline Aerosol, *J. Atmos. Chem.*,
570 40, 1–22, <https://doi.org/10.1023/A:1010657929716>, 2001.
- 571 Soussé-Villa, R., Jorba, O., Gonçalves Ageitos, M., Bowdalo, D., Guevara, M., and Pérez García-Pando, C.: A
572 Comprehensive Global Modelling Assessment of Nitrate Heterogeneous Formation on Desert Dust, *EGUsphere*, 2024,
573 1-53, <https://doi.org/10.5194/egusphere-2024-2310>, 2024.
- 574 Stelson, A. W. and Seinfeld, J. H.: Relative humidity and temperature dependence of the ammonium nitrate dissociation
575 constant, *Atmos. Environ.*, 16, 983-992, [https://doi.org/10.1016/0004-6981\(82\)90184-6](https://doi.org/10.1016/0004-6981(82)90184-6), 1982.
- 576 Sun, J., Zhang, M., and Liu, T.: Spatial and temporal characteristics of dust storms in China and its surrounding regions,
577 1960–1999: Relations to source area and climate, *J. Geophys. Res. Atmos.*, 106, 10325-10333,
578 <https://doi.org/10.1029/2000JD900665>, 2001.
- 579 Tan, S.-C., Shi, G.-Y., and Wang, H.: Long-range transport of spring dust storms in Inner Mongolia and impact on the
580 China seas, *Atmos. Environ.*, 46, 299-308, <https://doi.org/10.1016/j.atmosenv.2011.09.058>, 2012.
- 581 Trebs, I., Meixner, F. X., Slanina, J., Otjes, R., Jongejan, P., and Andreae, M. O.: Real-time measurements of ammonia,
582 acidic trace gases and water-soluble inorganic aerosol species at a rural site in the Amazon Basin, *Atmos. Chem. Phys.*,
583 4, 967-987, <https://doi.org/10.5194/acp-4-967-2004>, 2004.
- 584 Vasilakos, P., Russell, A., Weber, R., and Nenes, A.: Understanding nitrate formation in a world with less sulfate, *Atmos.*
585 *Chem. Phys.*, 18, 12765-12775, <https://doi.org/10.5194/acp-18-12765-2018>, 2018.
- 586 Wang, G., Zhang, R., Gomez, M. E., Yang, L., Levy Zamora, M., Hu, M., Lin, Y., Peng, J., Guo, S., Meng, J., Li, J.,
587 Cheng, C., Hu, T., Ren, Y., Wang, Y., Gao, J., Cao, J., An, Z., Zhou, W., Li, G., Wang, J., Tian, P., Marrero-Ortiz, W.,
588 Secrest, J., Du, Z., Zheng, J., Shang, D., Zeng, L., Shao, M., Wang, W., Huang, Y., Wang, Y., Zhu, Y., Li, Y., Hu, J.,



- 589 Pan, B., Cai, L., Cheng, Y., Ji, Y., Zhang, F., Rosenfeld, D., Liss, P. S., Duce, R. A., Kolb, C. E., and Molina, M. J.:
 590 Persistent sulfate formation from London Fog to Chinese haze, *Proc. Natl. Acad. Sci. U.S.A.*, 113, 13630-13635,
 591 <https://doi.org/10.1073/pnas.1616540113>, 2016.
- 592 Wang, J., Gui, H., An, L., Hua, C., Zhang, T., and Zhang, B.: Modeling for the source apportionments of PM₁₀ during
 593 sand and dust storms over East Asia in 2020, *Atmos. Environ.*, 267, 118768,
 594 <https://doi.org/10.1016/j.atmosenv.2021.118768>, 2021.
- 595 Wang, T., Liu, Y., Cheng, H., Wang, Z., Fu, H., Chen, J., and Zhang, L.: Significant formation of sulfate aerosols
 596 contributed by the heterogeneous drivers of dust surface, *Atmos. Chem. Phys.*, 22, 13467-13493,
 597 <https://doi.org/10.5194/acp-22-13467-2022>, 2022.
- 598 Weber, R. J., Guo, H., Russell, A. G., and Nenes, A.: High aerosol acidity despite declining atmospheric sulfate
 599 concentrations over the past 15 years, *Nat. Geosci.*, 9, 282-285, <https://doi.org/10.1038/ngeo2665>, 2016.
- 600 Xie, Y., Wang, G., Wang, X., Chen, J., Chen, Y., Tang, G., Wang, L., Ge, S., Xue, G., Wang, Y., and Gao, J.: Nitrate-
 601 dominated PM_{2.5} and elevation of particle pH observed in urban Beijing during the winter of 2017, *Atmos. Chem.*
 602 *Phys.*, 20, 5019-5033, <https://doi.org/10.5194/acp-20-5019-2020>, 2020.
- 603 Xin, K., Chen, J., and Tseren-Ochir, S.-E.: Formation mechanism and source apportionment of nitrate in atmospheric
 604 aerosols, *APN Sci. Bull.*, 13, 102-111, <https://doi.org/10.30852/sb.2023.2225>, 2023.
- 605 Xu, J. W., Lin, J., Luo, G., Adeniran, J., and Kong, H.: Foreign emissions exacerbate PM_{2.5} pollution in China through
 606 nitrate chemistry, *Atmos. Chem. Phys.*, 23, 4149-4163, <https://doi.org/10.5194/acp-23-4149-2023>, 2023.
- 607 Xu, L., Guo, H., Boyd, C. M., Klein, M., Bougiatioti, A., Cerully, K. M., Hite, J. R., Isaacman-VanWertz, G., Kreisberg,
 608 N. M., Knote, C., Olson, K., Koss, A., Goldstein, A. H., Hering, S. V., de Gouw, J., Baumann, K., Lee, S.-H., Nenes,
 609 A., Weber, R. J., and Ng, N. L.: Effects of anthropogenic emissions on aerosol formation from isoprene and
 610 monoterpenes in the southeastern United States, *Proc. Natl. Acad. Sci. U.S.A.*, 112, 37-42,
 611 <https://doi.org/10.1073/pnas.1417609112>, 2015.
- 612 Zhai, S., Jacob, D. J., Wang, X., Liu, Z., Wen, T., Shah, V., Li, K., Moch, J. M., Bates, K. H., Song, S., Shen, L., Zhang,
 613 Y., Luo, G., Yu, F., Sun, Y., Wang, L., Qi, M., Tao, J., Gui, K., Xu, H., Zhang, Q., Zhao, T., Wang, Y., Lee, H. C., Choi,
 614 H., and Liao, H.: Control of particulate nitrate air pollution in China, *Nat. Geosci.*, 14, 389-395,
 615 <https://doi.org/10.1038/s41561-021-00726-z>, 2021.
- 616 Zhang, C., Yan, M., Du, H., Ban, J., Chen, C., Liu, Y., and Li, T.: Mortality risks from a spectrum of causes associated



617 with sand and dust storms in China, *Nat. Commun.*, 14, 6867, <https://doi.org/10.1038/s41467-023-42530-w>, 2023.

618 Zhang, R., Wang, G., Guo, S., Zamora, M. L., Ying, Q., Lin, Y., Wang, W., Hu, M., and Wang, Y.: Formation of Urban
 619 Fine Particulate Matter, *Chem. Rev.*, 115, 3803-3855, <https://doi.org/10.1021/acs.chemrev.5b00067>, 2015.

620 Zhang, Y., Tang, L., Sun, Y., Favez, O., Canonaco, F., Albinet, A., Couvidat, F., Liu, D., Jayne, J. T., Wang, Z., Croteau,
 621 P. L., Canagaratna, M. R., Zhou, H.-c., Prévôt, A. S. H., and Worsnop, D. R.: Limited formation of isoprene epoxydiols-
 622 derived secondary organic aerosol under NO_x-rich environments in Eastern China, *Geophys. Res. Lett.*, 44, 2035-2043,
 623 <https://doi.org/10.1002/2016GL072368>, 2017.

624 Zhao, X., Huang, K., Fu, J. S., and Abdullaev, S. F.: Long-range transport of Asian dust to the Arctic: identification of
 625 transport pathways, evolution of aerosol optical properties, and impact assessment on surface albedo changes, *Atmos.*
 626 *Chem. Phys.*, 22, 10389-10407, <https://doi.org/10.5194/acp-22-10389-2022>, 2022.

627 Zheng, B., Cheng, J., Geng, G., Wang, X., Li, M., Shi, Q., Qi, J., Lei, Y., Zhang, Q., and He, K.: Mapping anthropogenic
 628 emissions in China at 1 km spatial resolution and its application in air quality modeling, *Sci. Bull.*, 66, 612-620,
 629 <https://doi.org/10.1016/j.scib.2020.12.008>, 2021.

630 Zheng, G., Su, H., Wang, S., Andreae, M. O., Pöschl, U., and Cheng, Y.: Multiphase buffer theory explains contrasts in
 631 atmospheric aerosol acidity, *Science*, 369, 1374-1377, <https://doi.org/10.1126/science.aba3719>, 2020.

632 Zheng, M., Xu, K., Yuan, L., Chen, N., and Cao, M.: Fine Particle pH and its Impact on PM_{2.5} Control in a Megacity of
 633 Central China, *Aerosol and Air Quality Research*, 22, <https://doi.org/10.4209/aaqr.210394>, 2022.

634